THE PUBLISHING HOUSE
OF THE ROMANIAN ACADEMY

PROCEEDINGS OF THE ROMANIAN ACADEMY, Series A,
Volume 14, Number 3/2013, pp. 211–218

3D IMAGING AND STATISTICS OF RED BLOOD CELLS IN MULTIPLE DEFORMATION STATES

Mona MIHAILESCU[*,**], Alexandru GHEORGHIU[**], Roxana-Cristina POPESCU**

[*] National Institute for Microtechnology, Bucharest, Romania
[**] "Politehnica" University of Bucharest, Bucharest, Romania
E-mail: mona_m@physics.pub.ro

In this paper we present our study regarding changes of human red blood cells (RBCs) immersed in solutions with different tonicity, monitored using digital holographic microscopy in order to connect their dimensions with the deformation states. We started with experimental images acquisition followed by our image processing procedure, which simultaneously provides information collected from more than one hundred cells from several images based on data from single cell level, and outputs are histograms after the main cell characteristics: minor radius, eccentricity, sphericity coefficient linked with the deformation states on three axes. It is also discussed how different digital filters are used for a better identification of the center and border of each cell.

Key words: digital holographic microscopy, red blood cells, deformation, tonicity.

1. INTRODUCTION

Fluxes through red blood cells (RBCs) membranes are very important in their life, in normal conditions, and especially, in order to treat or study different diseases, offering information about membrane quality [1–4]. Those fluxes influence cell morphology, structure and function, linked to the appropriate environmental characteristics. The osmolality of intra- and extracellular liquid are maintained in equilibrium even if its chemical composition differs. Increases in plasmatic osmolality of more than 2% are known as hyperosmolar states, respectively hypoosmolar, if the value decreases. In both cases, we can obtain information about cells membrane quality with direct consequence in the cell deformation. This behavior is important in RBCs passage through small capillaries, spleen functions [5], capillary wetting [6] and in several diseases, such as sickle cell anemia [7], hereditary spherocytosis [8], homozygous hereditary elliptocytosis [9], and malaria [10, 11]. Also, their deformability is important in blood preservation study [12]. From these reasons, more studies are needed to establish the relation between the three dimensional changes and the deformability state [13].

The most common technique used to study the RBCs deformability is ektacytometry [14–16], where a laser beam collects information from hundred of cells and forms one diffraction pattern in far field. New approaches have recently appeared [17, 18], to quantify a sample where fractions of cells with different deformation states are present. Our study is based on the deformation of the RBCs under different osmotic pressures, analyzed with the digital holographic microscopy (DHM) technique to obtain separately information about the deformation state of each cell. DHM is an innovative, non-destructive [19], marker free technique for living cells analysis; stem cells, breast cancer cells, bovine sperm head, or different micronic structures [20–22]. DHM offers quantitative information along the propagation axis with nanometric resolution. No scanning is required, i. e. DHM is suitable to investigate different phenomena: cells membrane vibrations, cells deformation in collagen matrix, cells motility, RBC-surface interaction, real-time determination of transmembranar water fluxes in neurons, cells dynamic evolution during microsurgery [23–28]. In this field, the reconstruction algorithm and the algorithms for objects identification have been recently improved [29–30].

We recorded holograms experimentally and the numerical reconstructions were made using an algorithm based on the diffraction scalar theory in Fresnel approximation. We will present the experimental images, their 3D reconstructions and our code developed in MATLAB which identifies the center and the borders of each cell, uses the simplest criteria for automatic cell recognition and exhibits statistical results after automatically reading the main characteristics of each cell from several images. This paper presents our statistical results based on data from single cell level, about each cell deformation on three axes, using DHM and the possibility to process automatically many images in order to make statistical analysis after the cells morphological changes. To deform cells more, we introduced them in a solution with higher concentration of glucose and induced a microflow. Statistical image analysis highlights the existence of different subpopulations with different deformation states.

2. EXPERIMENTAL RESULTS

Fresh blood samples from one volunteer (treated with no anticoagulant or buffer solution) were divided into three subsamples in order to observe the RBCs behavior in isotonic, hypotonic (diluted 1:2 with distilled water) and hypertonic (mixed 2:3 with 10% glucose) media. A drop from each sample was placed on a glass plate surface and a cover-slip was carefully placed over it, to avoid agglomeration of cells and to prevent the sample from drying during investigation procedures.

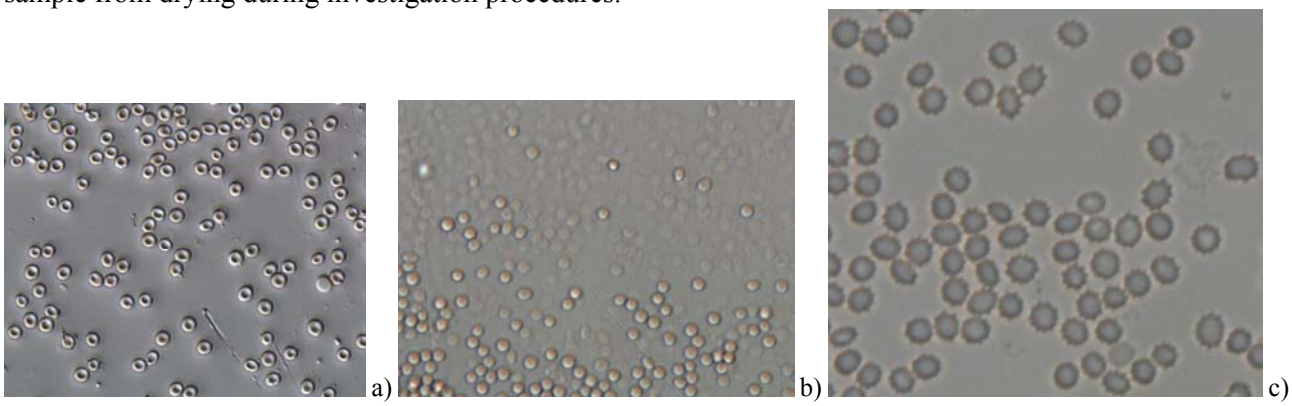

Fig. 1 – DIC images for RBCs in different media: a) isotonic; b) hypotonic; c) hypertonic.

Each sample was investigated experimentally using differential interference contrast (DIC) and DHM techniques. For DIC configuration we used Nikon equipment (Eclipse Ti-U, DS-Fi1 5megapixels CCD camera and dedicated software NIS Elements). In Fig. 1 are shown images recorded with RBCs in isotonic and hypotonic solutions; in Fig 1c) is shown an image of RBCs in hypertonic solution, recorded at high resolution, in order to emphasize the jagged edges.

For sample visualization with DHM technique, we used an off-axis geometry set-up, based on the Mach-Zehnder interferometer in the transmission mode arrangement (almost all biological samples are transparent in visible range), where the investigated object was placed in one arm. Identical microscope objectives (40x) were used in the reference and object arms, in order to obtain the same wave-front curvature in the CCD plane. A single recorded hologram (an intensity image) on the CCD sensor is enough to reconstruct the phase shift introduced by the transparent sample in the optical path. Neutral density filters were used to adjust light intensity for a proper visibility of the holograms recorded by the CCD (Pike F421 with Kodak sensor 2048 × 2048pixels, pixel pitch Δx = 7.4μm, acquisition rate of 16fps at full resolution). Starting from this pitch, we chose the minimum inter-fringe of $9\Delta x$, which corresponds to a spatial frequency of $1/(9\Delta x)$, to be in accordance with the maximum spatial frequency established by the Nyquist-Shannon sampling theorem of $1/(2\Delta x)$. In Fig. 2 are shown some experimentally recorded holograms, using a He-Ne laser (double stabilized from Spectra Physics) on a CCD sensor. It can be easily observed that the diffraction pattern from each cell is superposed with the reference wave (we have the circular diffraction maximum and minimum, and also the linear interference fringes). Starting with these experimentally recorded holograms, we used an algorithm for object image reconstruction and aberration compensation [31–35].

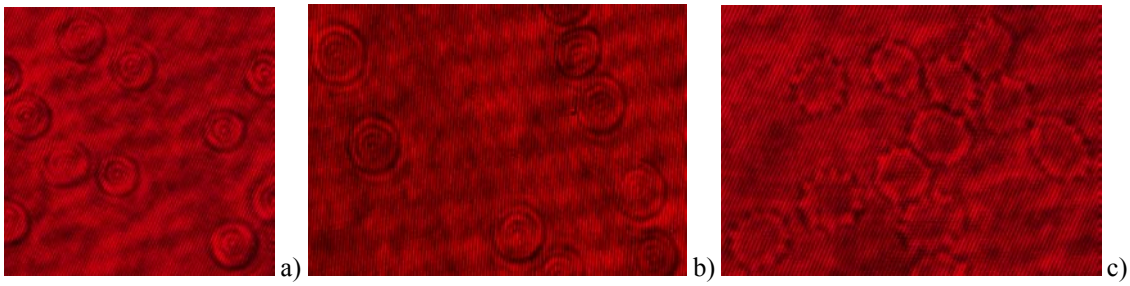

Fig. 2 – Holograms recorded in DHM for RBC situated in a) isotonic, b) hypotonic, c) hypertonic solutions.

The sample images corresponding to the phase shift introduced by each cell in the optical path, are given in Fig. 3. These images are different from those shown as holograms because, for statistical reasons, we recorded more than ten images for each situation. Again, for cells situated in the hypertonic solution, we enlarged a detail in order to observe the star shape of the RBCs.

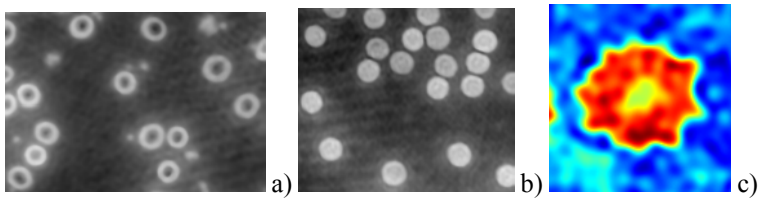

Fig. 3 – Images reconstructed from holograms for RBCs situated in a) isotonic, b) hypotonic, c) hypertonic solutions.

In Fig. 4 are shown few reconstructed images using a 3D representation. The phase shift is transformed in false colors which are proportional with thickness values within the sample (the proportionality constant depends linearly on the difference between the refractive index of the surrounding medium and the refractive index of the cell which are both assumed to be constant for a given sample).

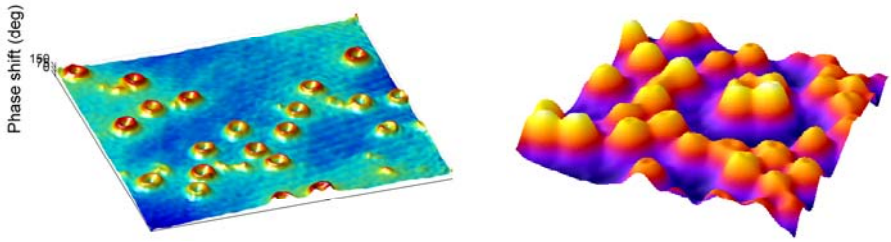

Fig. 4 – 3D reconstructions for cells situated in isotonic (left) and hypotonic (right) solutions.

In Fig. 5 are presented two profiles (obtained from experimental reconstructions) for a) a RBC in isotonic medium and b) a RBC in hypotonic medium. We use the sphericity coefficient [36] defined theoretically as the ratio between the values of the minimum phase shift in the middle of the cell and the maximum phase shift within the whole cell. It gives information about the cells potential related to the deformation on the perpendicular axis of the cells resting plane. We implemented a numerical algorithm, which automatically identifies the position of the centroid of each cell (explained in section 3.). Starting from this point, we computed the radial gradient of the cell. The aim was to observe two behaviors for two different values of the slope, until the maximum value for phase is found: 1) for small values of gradient and slope, corresponding to the bottom of the concavity, 2) for greater values of gradient and slope, corresponding to the walls of the concavity. Based on these values, we separated two regions: 1) the bottom of the concavity and 2) its ridge. Then, the algorithm calculates the minimum phase shift p_m as a medium value of the bottom of the concavity and the maximum phase shift p_M as a medium value of the concavity ridge. Both values are computed relative to the background value set to zero. Their ratio is equal to the ratio between the cell thicknesses in the same regions because the difference between the refractive indices of the cell and the surrounding media is constant for a given sample. From all these images, we observe that the RBCs in isotonic medium are circular cells of 7.8 μm diameter with a middle concavity. In physiologic

states, in isotonic solution, with the same osmotic pressure as plasma, RBCs tend to maintain the biconcave disc form and its integrity. In the case of the sample immersed in hypertonic solution, we observe that RBCs transform into star shaped cells, with jagged margins. In hypotonic solution, the specimen presents almost spherically shaped cells, with a small central concavity or without it.

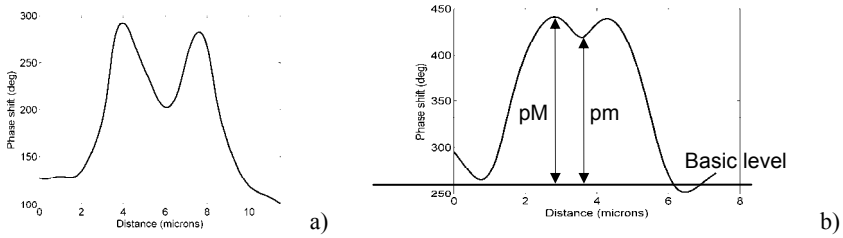

a) b)

Fig. 5 – Profiles through cells situated in: a) isotonic; b) hypotonic solutions.

3. NUMERICAL RESULTS

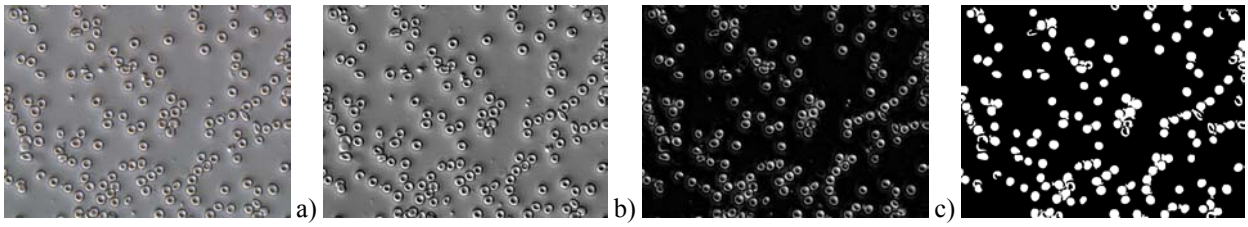

a) b) c) d)

Fig. 6 – a) Experimental image; b) the same image with enhanced contrast;
c) image after background has been removed d) Binary image.

In order to obtain data regarding cell properties (approximately 100 cells from around six images for each type of subsample), an automated image analysis procedure based on image processing techniques is required [37, 38]. We started with a grayscale image and used two MATLAB functions for contrast adjustment: '*imadjust*', which maps intensity values in the original image to new values, so that 1% of the data is saturated at low and high intensities, and '*histeq*', which equalizes the histogram of the image (Fig. 6a,b). Next, we identified the background and subtracted it from the image (erode and dilate the image using a disk-shaped structuring element having relatively the same size as a cell (Fig. 6c)). To convert the image to a binary (Fig. 6d) the threshold value was automatically chosen, however for some images, it is necessary to introduce an empirically determined value (but we disclaim those images). This 'raw' image must be processed further as it most often contains fragments from various objects. For images with a low contrast (Fig. 7a), an alternative procedure was used. The regional maxima in the original image were identified and the color scheme was inverted (Fig. 7b). The next step was to remove unwanted elements (the algorithm selects which elements to remove based on their size or shape, which can be irregular) and to fill donut-shaped objects (Fig. 7c).

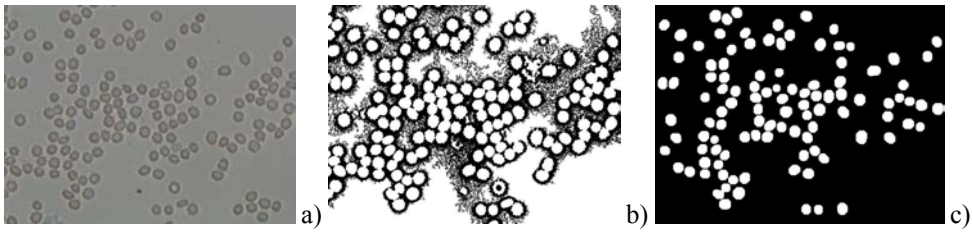

a) b) c)

Fig. 7 – a) Experimental image; b) inverted regional maxima identification; c) binary image.

For images experimentally obtained using DHM (Fig. 8a) we developed a more general algorithm, which can be applied to a wide range of images, to produce satisfactory statistical results. Since pixel values now corresponded to phase shifts, the problem was reduced to identifying local maxima, using an extended

maxima transform, applied to the contrast-enhanced image and produced a binary image with a greatly reduced number of fragments (Fig. 8b). The next steps are to fill donut-shaped elements (Fig. 8c) and filter out objects having an area greater or less than one standard deviation with respect to the mean (Fig. 8d). This type of filtering proved to be sufficient, since the extended maxima transform eliminated most of the noise from the image and only few unwanted elements remained.

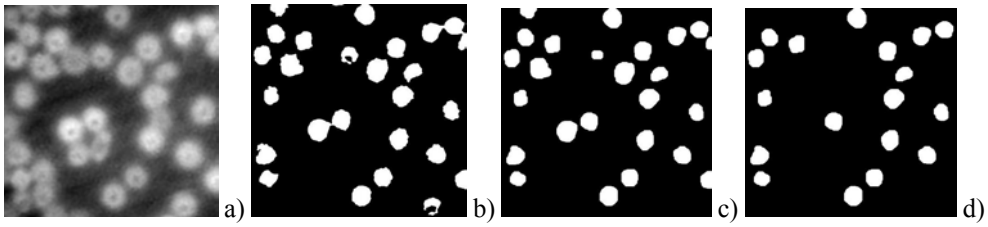

Fig. 8 – a) Experimental image; b) regional maxima identification and obtaining binary images; c) eroded and dilated objects to separate adjacent cells; d) remaining objects after statistic filtration.

A problem which arises is that neighboring cells can appear as a single object in the binary image instead of two or more separate objects. We noticed this as ellipses, joined together by thin bridges. To solve this problem we eroded and then dilated the binary image in order to remove the bridging elements and then restore the cells to their original sizes. This procedure is effective when the structuring element used is comparable in size to the cells (compare Fig. 8b and 8c). Since cells had the same relative size in images taken at the same resolution, there was no need to change the radius of the disk-shaped structuring element.

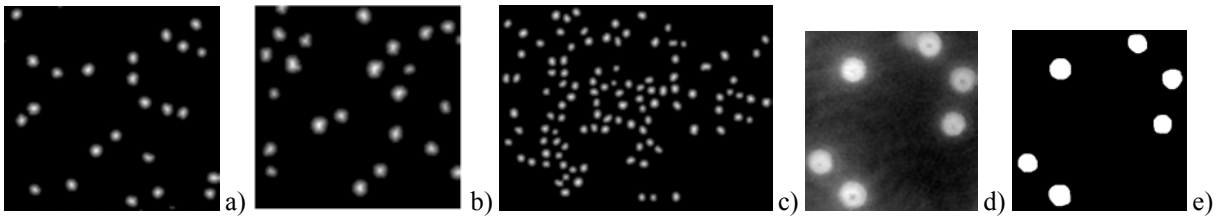

Fig. 9 – Distance transform applied on images obtained with cells in different media: a) isotonic; b) hypotonic; c) hypertonic; d) reconstructed image obtained in DHM for cells in hypotonic medium; e) its binary image obtained directly.

The final step was to apply a distance transform (Fig. 9a, b, c), to identify the various objects present in the image and to determine properties such as position of the centroids, eccentricity, area and minor radius. In images in which cells are isolated and the background is relatively uniform, we directly transformed reconstructed images to black and white, without intermediate steps (contrast enhancement, background elimination and shapes filtering or filling), as seen in Fig. 9d and 9e, with cells in hypotonic medium.

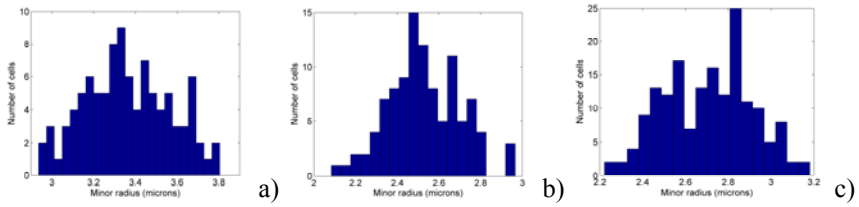

Fig. 10 – Histograms after minor radius for cells in: a) isotonic; b) hypotonic; c) hypertonic media.

Finally, we determined various properties for the remaining cells and constructed histograms with the statistical data gathered (Fig. 10). The remaining objects were the best identified cells. The images from DHM gave the phase shifts introduced by the cells and we computed their eccentricity, minor radius, sphericity coefficient, parameters which gave complete information about each cell deformation on three axis. In this case, we turned to images with initial contrast and background with identified cells borders. For a better visualization, in order to compare the results, these histograms were fitted using '*cftool*' in MATLAB (Fig. 11). The compared parameters gave information about 3D deformability: in the transverse plane (eccentricity and minor axis) and along the propagation axis (sphericity coefficient).

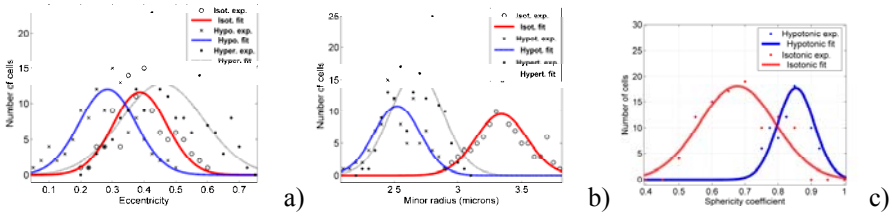

Fig. 11 – Comparative behavior for different properties of cells: a) eccentricity; b) minor radius; c) sphericity coefficient.

To deform the cells more, we increased the plasmatic osmolality and we tilt the sample with a small angle, having different impacts on RBCs behavior. Inside, cells were in a disordered motion. In the images that were experimentally recorded in DIC and DHM, it can be seen that cells are deformed in different ratios (see Fig. 12a for a DIC image, 12b for a hologram and 12c, d for cropped regions from the reconstructed images).

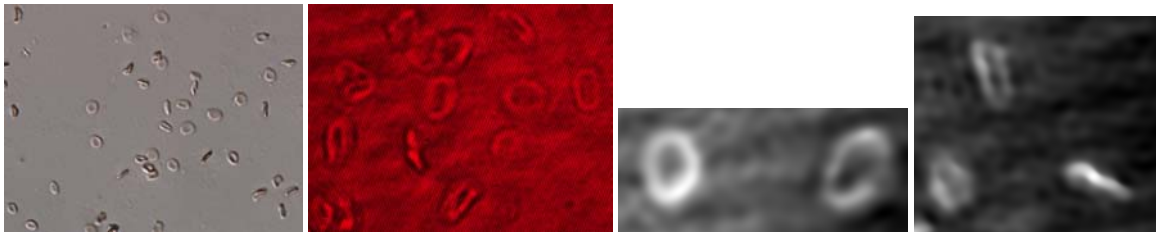

a) b) c) d)

Fig. 12 – Images of the cells in motion: a) DIC; b) a hologram acquired in DHM; c), d), e), f) different reconstructions.

These images were processed following the steps described above and the resulting histograms matched the simple visual observation: the existence of subpopulations after eccentricity and minor radius (Fig. 13a, b). The identified objects (cells) in each image, which have the minor radius less than two microns and eccentricity more than 0.9, correspond to the rotated cells, where their thickness is available for measurements. They will be filtered and removed from the statistical analysis. These results demonstrate the validity of the image processing algorithm, because it accurately separates subpopulations with different characteristics.

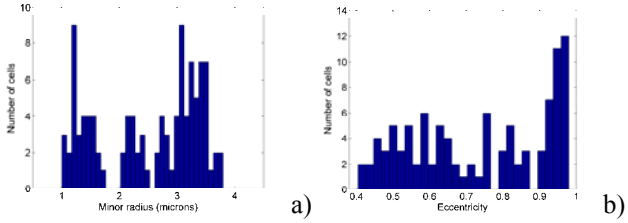

Fig. 13 – Histograms for cells in microflow in hypertonic medium after: a) minor radius; b) eccentricity.

4. CONCLUSIONS

Experimental images were recorded using subsamples which contained RBCs situated in extracellular media with different osmolalities. They were consistent with the theory of osmotic phenomena in hypertonic and hypotonic media, where an internal pressure is exercised on the RBC membrane. The cells swelling in hypotonic and shrinking in hypertonic media, provided information about the chemical quality of the membrane and the cell deformability potential, which are important properties in cellular functions and an important indicator for different diseases. Using this method, we can obtain experimentally different values for the applied stress on the RBC membrane. In order to obtain statistical information about different features of each sample, based on the analysis of single cell level, we developed a code in MATLAB comprising of the following steps: inverted regional maxima identification, eroding in order to remove bridges between

adjacent cells and distance transform for cell centroid identification. Once the cells have been identified, the program proceeds to compute various properties of these objects. The histograms produced once the procedure ends, resulted after automatically processing several images, were fitted with Gaussian functions, in order to compare different cell characteristics (eccentricity, minor radius, sphericity coefficient) in each medium. Using information about the sphericity coefficient of cells in hypotonic medium (available only from DHM measurements), the deformability along the propagation axis is available. We introduced a more accurate procedure, digitally implemented, to compute the sphericity coefficient. The evolution of the eccentricity and minor radius values offers information about deformability in the transversal plane.

Our statistical results are in accordance with the osmotic theory and with other measurements accurately done using a related optical technique [39]. The RBCs situated in hypotonic media have smaller values for eccentricity because their projection becomes more circular after swelling; and smaller values for minor radius due to surface tension which causes cells to increase in height. The sphericity coefficient is also in accordance with this rising, while the semi-high width of its gaussian fitting curve indicates that cells in hypotonic media tend to be more similar each to another. The RBCs situated in hypertonic medium have higher values for eccentricity and lower values for minor radius due to their shrinking. This is a complete statistical image about the 3D deformability based on data from single cell level. The experimental results followed by the image processing steps show that these properties can be used to classify the RBCs in different states of deformability. We also developed a method to obtain highly deformed cells in transversal plane after we induced a small tilt of the subsample with cells in hypertonic solution with highest concentration. These images are processed and the algorithm accurately separates the subpopulations related with the deformability potential on a transversal plane. We can conclude that this method is the first stage in RBCs subpopulations recognition from the same sample (image) which have different deformability states. The experimental procedure, described here, followed by the digital steps in image processing, automatically gives statistical information about the morphological characteristics of deformed cells, used to discriminate RBCs in different states of deformability. These procedures are suitable and can be also used in order to characterize the effects of different therapeutic agents on the cellular 3D deformability, using digital holographic microscopy for quantitative information along the propagation axis with nanometric accuracy.

ACKNOWLEDGEMENTS

The research presented in this paper is supported by the Sectorial Operational Program for Human Resource Development financed by the European Social Fund and by the Romanian Government under the contract no. POSDRU/89/1.5/S/63700. The equipments used in these experiments were acquired using funds from the Romanian contract 4/CP/I/2007-2009. One of the authors (M.M.) wants to thank to M. Scarlat, D. Stan and T. Savopol for useful advices.

REFERENCES

1. M.P. GAGNON, P. BISSONNETTE, L.M. DESLANDES, B. WALLENDORFF, J. Y. LAPOINTE, *Glucose Accumulation Can Account for the Initial Water Flux Triggered by Na^+/Glucose Cotransport*, Biophys J., **86**, pp. 125–133, 2004.
2. R.J. NAFTALIN, *Water Transport with Glucose in GLUT2 and SGLT,* Biophys J., **94**, pp. 3912–3923, 2008.
3. M. van der HEIJDEN, J. VERHEIJ, G. van AMERONGEN, J. GROENEVELD, *Crystalloid or colloid fluid loading and pulmonary permeability, edema, and injury in septic and nonseptic critically ill patients with hypovolemia*, Crit. Care Med., **37**, pp. 1275–1281, 2009
4. S.K. CRIBBS, G.S. MARTIN, *Fluid balance and colloid osmotic pressure in acute respiratory failure: optimizing therapy*, Exp. Rev. Respir. Med., **3**, pp. 651–62, 2009
5. I. SAFEUKUI, P.A. BUFFET, G. DEPLAINE, S. PERROT, V. BROUSSE, A. NDOUR, M. NGUYEN, O. MERCEREAU-PUIJALON, P.H. DAVID, G. MILON, N. MOHANDAS, *Quantitative assessment of sensing and sequestration of spherocytic erythrocytes by human spleen: implications for understanding clinical variability of membrane disorders*, Blood, **2**, pp. 424-430, 2012.
6. R. ZHOU, J. GORDON, A.F. PALMER, H.-C. CHANG*, Role of Erythrocyte Deformability During Capillary Wetting*, Biotech. and Bioeng., **93**, pp. 201-21, 2006.
7. G.R. SERJEANT, B.E. SERJEANT, P.F. MILNER, *The Irreversibly Sickled Cell; a Determinant of Haemolysis in Sickle Cell Anaemia*, British J. of Haemat., **17**, pp. 527–533, 1969.
8. S. PERROTTA, P.G. GALLAGHER, N. MOHANDAS, *Hereditary spherocytosis*, The Lancet, **372**, pp. 1411–1426, 2008.

9. G. TEBERNIA, N. MOHANDAS, S.B. SHOHET, *Deficiency of skeletal membrane protein band 4.1 in homozygous hereditary elliptocytosis. Implications for erythrocyte membrane stability*, J. Clin. Invest., **68**, pp. 454–460, 1981.
10. H. KONDO, Y. IMAI, T. ISHIKAWA, K. TSUBOTA, T. YAMAGUCHI, *Hemodinamic analysis of microcirculation in malaria infection*, Annals of Biomed. Eng., **37**, pp. 702–709, 2009.
11. B.M. Cooke, N. MOHANDAS, R.L. COPPEL, *The malaria-infected red blood cell: Structural and functional changes*, Adv. in Parasit., **50**, pp. 1–86, 2001.
12. J. WU, Y. LI, D. LU, Z. LIU, Z. CHENG, L. HE, *Measurement of the membrane elasticity of red blood cell with osmotic pressure by optical tweezers*, Cryo Lett**.**, **30**, pp. 89–95, 2009.
13. G. CHIOCCHIA, R. MOTAIS, *Effect of catcholamines on deformability of red cells from trout: relative roles of cyclic amp and cell volume*, J. of Physiol., **412**, pp. 321–332, 1989.
14. W. GRONER, N. MOHANDAS, M. BESSIS, *New Optical Technique for Measuring Erythrocyte Deformability with the Ektacytometer,* Clin. Chem., **26**, pp. 1435–1442, 1980.
15. G.J. STREEKSTRA, A.G. HOEKSTRA, E.-J. NIJHOF, R.M. HEETHAAR, *Light scattering by red blood cells in ektacytometry: Fraunhofer versus anomalous diffraction*, Appl. Opt., **32**, pp. 2266–2272, 1993.
16. S. SHIN, Y.H. KU, M.S. PARK, S.Y. MOON, J.H. JANG, J.S. SUH, *Laser-diffraction slit rheometer to measure red blood cell deformability*, Rev. Sci. Instrum., **75**, pp. 559–561, 2004.
17. G.J. STREEKSTRA, J.G.G. DOBBE, A.G. HOEKSTRA, *Quantification of the fraction poorly deformable red blood cells using ektacytometry*, Opt. Express., **18**, pp. 14173–14182, 2010.
18. M. MIHAILESCU, J. COSTESCU, *Diffraction pattern study for cell type identification*, Opt. Express, **20**, pp. 1465–1474, 2012.
19. Z. EL-SCHISH, A. MOLDER, M. SEBESTA, L. GISSELSSON, K. ALM, GJÖRLOFF WINGREN, *Digital holographic microscopy- innovative and non-destructive analysis of living cells*, Microsc. Sci. Tech. Appl. Educ., FORMATEX 2010.
20. I. MOON, B. JAVIDI, *Three-dimensional identification of stem cells by computational holographic imaging*, J. R. Soc. Interface, **4**, pp. 305–313, 2007.
21. P. MEMMOLO, G. DI CAPRIO, C. DISTANTE, M. PATURZO, R. PUGLISI, D. BALDUZZI, A. GALLI, G. COPPOLA, P. FERRARO, *Identification of bovine sperm head for morphometry analysis in quantitative phase-contrast holographic microscopy*, Opt. Express, **19**, pp. 23215–23226, 2011.
22. Q. WEIJUAN, C.O. CHOO, Y. YINGJIE, A. ASUNDI, *Microlens characterization by digital holographic microscopy with physical spherical phase compensation*, Appl. Opt., **49**, pp. 6448–6454, 2010.
23. B. RAPPAZ, A. BARBUL, A. HOFFMANN, D. BOSS, R. KORENSTEIN, C. DEPEURSINGE, P.J. MAGISTRETTI, P. MARQUET, *Spatial analysis of erythrocyte membrane fluctuations by digital holographic microscopy*, Blood Cells Mol. Dis., **3**, pp. 228–232, 2009.
24. K. AZARTASH, E. GRATTON, *Obtaining Quantitative Information on the Cell-induced Deformation of Collagen with Digital Holographic Microscopy*, Biophys. J., **96**, pp. 297a, 2009
25. F. DUBOIS, C. YOURASSOWSKY, *Digital holographic microscopy for the three-dimensional dynamic analysis of* in vitro *cancer cell migration*, J. Biomed. Opt., **1**, pp. 054032, 2006.
26. I. BERNHARDT, L. IVANOVA, P. LANGEHANENBERG, B. KEMPER, G. VON BALLY, *Application of digital holographic microscopy to investigate the sedimentation of intact red blood cells and their interaction with artificial surfaces*, Bioelectrochem., **73**, pp. 92–96, 2008.
27. P. JOURDAIN, N. PAVILLON, C. MORATAL, D. BOSS, B. RAPPAZ, C. DEPEURSINGE, P. MARQUET, P.J. MAGISTRETTI, *Determination of Transmembrane Water Fluxes in Neurons Elicited by Glutamate Ionotropic Receptors and by the otransporters KCC2 and NKCC1: A Digital Holographic Microscopy Study*, J. of Neurosci., **31**, pp. 11846–11854, 2011.
28. L. YU, S. MOHANTY, J. ZHANG, S. GENC, M. K. KIM, M. W. BERNS, Z. CHEN, *Digital holographic microscopy for quantitative cell dynamic evaluation during laser microsurgery*, Opt. Express, **17**, pp. 12031–12038, 2009.
29. C. YUAN, G. SITU, G. PEDRINI, J. MA, W. OSTEN, *Resolution improvement in digital holography by angular and polarization multiplexing* Appl. Opt., **50**, pp. B6–B11, 2011
30. A. EL MALLAHI, F. DUBOIS, *Dependency and precision of the refocusing criterion based on amplitude analysis in digital holographic microscopy*, Opt. Express, **19**, pp. 6684–6698, 2011.
31. E. CUCHE, P. MARQUET, C. DEPEURSINGE, *Simultaneous amplitude and quantitative phase contrast microscopy by numerical reconstruction of Fresnel off-axis holograms*, Appl. Opt., **38**, pp. 6994–7001, 1999.
32. T. COLOMB, E. CUCHE, F. CHARRIÈRE, J. KÜHN, N. ASPERT, F. MONTFORT, P. MARQUET, C. DEPEURSINGE, *Automatic procedure for aberration compensation in digital holographic microscopy and applications to specimen shape compensation*, Appl. Opt., **45**, pp. 851–863, 2006.
33. T. MONTFORT, F. CHARRIÈRE, T. COLOMB, E. CUCHE, P. MARQUET, C. DEPEURSINGE, *Purely numerical compensation for microscope objective phase curvature in digital holographic microscopy: influence of digital phase masks position*, J. Opt. Soc. Am., A **23**, pp. 2944-2953, 2006.
34. T. COLOMB, N. PAVILLON, J. KÜHN, E. CUCHE, C. DEPEURSINGE, Y. EMERY, *Extended depth-of-focus by digital holographic microscopy*, Opt. Lett., **35**, pp. 1840–1842, 2010.
35. *** http://www.lynceetec.com/content/view/497/193/ 15 November 2012.
36. T. TISHKO, T. DMITRY, T. VLADIMIR, *Holographic Microscopy of Phase Microscopic Objects*, World Scientific, 2011.
37. I. MOON, B. JAVIDI, F. YI, D. BOSS, P. MARQUET, *Automated statistical quantification of three-dimensional morphology and mean corpuscular hemoglobin of multiple red blood cells*, Opt. Express, **20**, pp. 10295–10310, 2012.
38. M. MIHAILESCU, M. SCARLAT, A. GHEORGHIU, J. COSTESCU, M. KUSKO, I.A. PAUN, E. SCARLAT, *Automated imaging, identification, and counting of similar cells from digital hologram reconstructions*, Appl. Opt., **50**, pp. 3589–3597, 2011.
39. YONGKEUN PARK, *Pathophysiology of human red blood cell probed by quantitative phase microscopy*, Ph. D. Thesis.

Received February 11, 2013